Growth Modelling Promoting Mechanical Stimulation of Smooth Muscle Cells of Porcine Tubular Organs in a Fibrin-PVDF Scaffold

Minh Tuấn Dương, Volker Seifarth, Ayşegül Artmann, Gerhard M. Artmann and Manfred Staat

1 Introduction

In modern industrial countries, live expectancy has increased due to improved medical standards, hence, a whole pallete of organ abnormalities, disorders or trauma can be cured [1, 2]. However, organ maldevelopment and injury of the genitourinary tract and especially the ureters and urethras can result in severe complications that may badly influence quality of life. Reconstructive surgery and tissue replacements like tubularized intestine segments for ureter reconstruction often bring about for example stricture formation, fistula, stenosis, obstruction, metaplasia, hydro-(neoureter) nephrosis, mucous production and/or chronic inflammatory reactions [3, 4].

Furthermore, there is a demand for developing alternative reconstruction methods in the field of urology. Novel promising techniques in reconstructive surgery deal with Tissue Engineering (TE) procedures on which for example autologous cells, taken from bladder biopsies, are seeded on tubular scaffolds to create bio-artificial tissue constructs [5–7]. In addition, a bioreactor may be a promising technology to generate also an almost functional tissue substitute in

M. T. Dương (✉) · V. Seifarth · A. Artmann · G. M. Artmann · M. Staat
Institute for Bioengineering, University of Applied Sciences Aachen, Heinrich-Mußmann-Str. 1, 52428 Jülich, Germany
e-mail: minhtuan.duong9@gmail.com

G. M. Artmann
e-mail: g.artmann@gmx.net

M. T. Dương
University of Erlangen-Nuremberg, Immerwahrstraße 1, 91058 Erlangen, Germany

M. T. Dương
Hanoi University of Science and Technology, No. 1, DaiCoViet Road, Hanoi, Vietnam

G. M. Artmann et al. (eds.), *Biological, Physical and Technical Basics of Cell Engineering*, https://doi.org/10.1007/978-981-10-7904-7_9

mimicking the physiological surrounding of the tissue of interest [8] in which the bioreactor gives a stimulus to the cells to copy the nature. For urological TE purposes, Qiang Fu et al. demonstrated that mechanical extension stimulation can improve the viability of adipose derived stem cells (ADSCs) induced to differentiate into SMCs and form a muscular tube of urethral TE [9]. However, a cellular alignment in both circular and longitudinal directions could not yet be achieved.

Moreover, computational growth modelling is often adopted to predict the tendency of cell growing or atrophying under loading conditions. For soft tissue growth, density is mostly considered to be constant, meanwhile changes take place in volume. The decomposition of the total growth deformation into a growth part and an elastic part, applied to a material characterized by a 3D (three-dimensional) simple Fung-type potential [10]. Moreover, the multiplicative decomposition of the deformation gradient into elastic deformation and growth part for isotropic, transversely isotropic and orthotropic biomaterials were presented in the framework of finite deformation [11]. The idea for isotropic growth for an isotropic material was then realized by [12] with their algorithmic realisation in a finite element setting in which the isotropic stretch ratio is introduced as internal variable at the integration point level. Subsequently, this idea was applied to analyse the isotropic growth for arterial walls and in-stent restenosis related to atherosclerosis [13]. However, the material describing the arterial wall is the neo-Hookean which is not realistic because arteries are anisotropic [14]. In this paper, we first investigate the smooth muscle cells in a tubular fibrin scaffold by mechanical stimulation and then computational growth modelling is analysed with two growth models, which are isotropic growth and transversely isotropic growth for isotropic muscle cells in order to accurately simulate and observe behaviour of cells.

2 Mechanical Stimulation

2.1 Materials and Methods

2.1.1 Cell Isolation

Smooth muscle cells were isolated from porcine bladders that were obtained from a local abattoir, dissected and sliced into pieces of about 1 mm^3 as in [15]. Tissue samples (20) were placed in T75 flasks (Nunc, Germany) and incubated with a standard cell culture medium (provided by Invitrogen and Sigma Aldrich, Germany). Medium was changed regularly after three to four days and cells were passaged up to four times, before they were applied in fibrin scaffolds.

2.1.2 Fibrin Gel Preparation

Fibrinogen from human plasma (Merck Millipore, Germany) was prepared as described in [16]. Fibrinogen was dissolved in double distilled water (ddH_2O) at 25 mg/mL, before it was dialyzed over night against Trizma buffered saline (TBS), using a dialysis membrane with a cut off of 6000–8000 MW (Carl Roth, Germany). After sterile filtration, the fibrinogen concentration was determined with a spectrophotometer (Jasco, Germany) at 280 nm and an extinction coefficient of 1.55 [17].

Fibrin gels (n = 14) were prepared with 3 mL fibrinogen (12.5 mg/mL), 2.1 mL TBS that include 3×10^7 cells, 450 µL thrombin (40 IU/mL) and 450 µL calcium chloride (50 mM). In the end, a fibrinogen concentration of 6.25 mg/mL was achieved with a cell count of 5×10^6 cells/mL. Biohybrids were cultured with the standard cell culture medium supplemented with 1 mM L-ascorbic acid 2-phosphate (Sigma Aldrich, Germany) to enhance the tissue and collagen secretion and with 0.5 mg/mL tranexamic acid (Pfizer, Germany) to prevent fibrinolysis [18, 19].

2.1.3 Scaffold Preparation and Cell Seeding

Figure 1 shows a casting mould for the preparation of a tubular composite scaffold made up of fibrinogen and polyvinylidene fluoride (PVDF). The PVDF mesh (RWTH Aachen, Germany) formed the inner layer of the tubular structure. This mould was produced out of Teflon and polyoxymethylene (POM) and was manufactured at Aachen University of Applied Sciences, Germany.

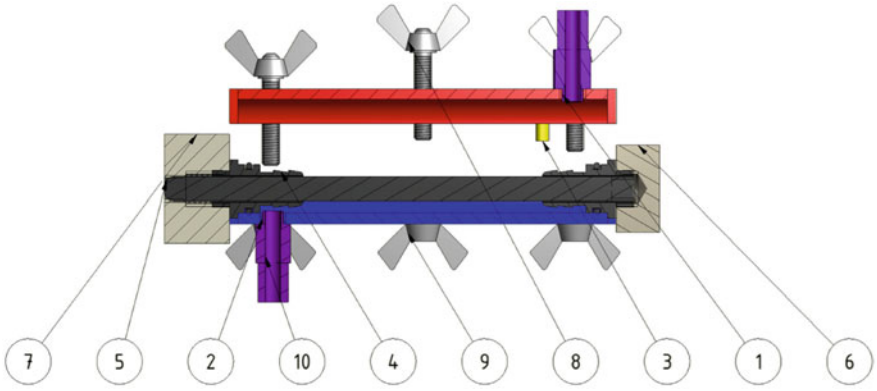

Fig. 1 Casting mould for composite biohybrids consisting of: top (*1*), bottom (*2*), pins for positioning (*3*), fittings (*4*), central rod (*5*), front cap (*6*), end cap (*7*), wing bolts/nuts (*8*)/(*9*) and Luer adapters (*10*) [21]

The fibrinogen solution and the cell suspension were injected into the mould by a two-chamber application system (Medmix, Switzerland). The polymerization inside the mould starts within several seconds and results in a 2 mm thick and 75 mm long tubular structure with an inner diameter of 6 mm. The biohybrid was transferred into the bioreactor after 45 min of polymerization at room temperature.

2.1.4 Mechanotransduction

A kyphoplasty catheter (Joline, Germany) was inserted into the lumen of the biohybrid in order to mimic a urine drop. The catheter was inflated by a syringe pump and was pulled through the tube by a linear actuator. The mechanical experimental stimulator system was partially manufactured by the HITEC Zang GmbH (Herzogenrath, Germany). Subsequently, the catheter was deflated and pushed forward, again. This mechanical stimulation was performed with a frequency of 0.015 Hz. The inflation of the catheter followed a sigmoidal waveform as it is depicted in Fig. 2 with a maximal strain of 20% [20, 21].

2.1.5 Histological Analysis

Tissue fragments were fixed in Carnoy's fluid for at least 8 h, before they were dehydrated and embedded in paraffin. Dehydration, embedding, slicing in 5 µm sections and haematoxylin and eosin (H&E) staining were performed.

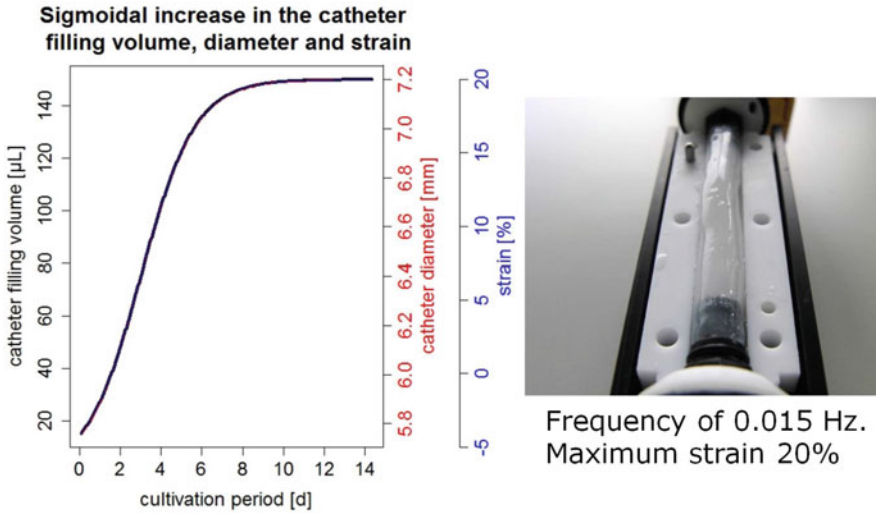

Fig. 2 A sigmoidal waveform and a casting of scaffold [21]

The analysis of the alignment of cells in histological cross sections and scanning electron microscopic pictures from the outer surface of the tubes was performed with LabVIEW (National Instruments, USA). Cellular and structural orientations were analysed according to the size of the interquartile ranges.

2.1.6 Biochemical Analysis

Diffusion experiments were performed as previously described in [15]. Samples of Krebs buffer with a volume of 1 mL were taken after 0.5, 1, 1.5, 2, 3, 4, 5, 6, 7, 8 h. The sample volume was replaced by fresh buffer and the concentration of urea and creatinine were then determined (Uniklinik RWTH Aachen, Germany).

2.1.7 Mechanical Properties

Mechanical properties were analysed by the rupture pressure of the tissue fragments. A chamber was constructed for inflation test at bursting pressure (Aachen University of Applied Sciences, Germany).

Five to ten cm long tubular structures were sliced longitudinally and were arranged in the pressure chamber in a way that an increasing pressure was applied onto the extraluminal surface of the biohybrids. A syringe pump was controlled and the data acquisition were performed with an interface (HiTec Zang GmbH, Germany).

2.2 Results and Discussion

Figure 2 shows homogeneous, bubble free 75 mm long fibrin-VDF composite prosthesis that polymerized for 45 min in the casting mould at room temperature [22]. For mechanical stability, the rupture pressure revealed that there are no significant differences between mechanically stimulated and unstimulated prosthesis. Table 1 indicates that there was a tendency to increasing mechanical stability for stimulated prostheses. A similar tendency was observed for extended incubation periods. The rupture pressure increased after two weeks of incubation and with mechanical stimulation. On cellular orientation, histological cross sections stained with HE show an orientation of cells for stimulated prosthesis in comparison to untrained prosthesis. This can be observed due to elongated cell morphologies, see Fig. 3. Scanning electron microscopy from the outer tubular surface exposed that mechanically stimulated tissues show a preferred orientation of cells along the tubular structure of the prosthesis [8]. Obviously, the intensity of mechanical stimulation is dependent on various parameters and different models: the applied cell type, cell source, cell passage as well as in the experimental setup. Nevertheless, it is seen to be stress level and cell type specific.

Table 1 Bursting pressure[21]

Incubation period	$P_{untrained}$ [mbar]	$P_{trained}$ [mbar]
One week	1210 ± 310	1530 ± 50
Two weeks	1450 ± 530	2120 ± 200

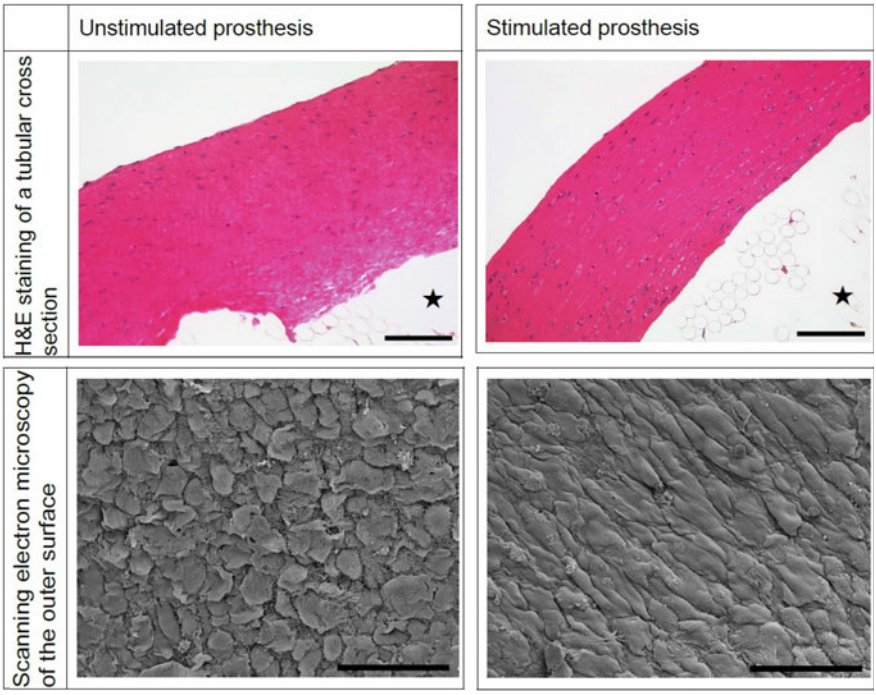

Fig. 3 Morphological appearance of mechanically unstimulated (left) and stimulated (right); H&E staining [21]

Tissue engineering as multidisciplinary field in science might lead to new technologies for the replacement of defect genitourinary tract organs. For that reason, different cultivation methods as well as scaffold materials are continuously tested and developed. The application of mechanical forces plays a crucial role for the tissue generation and orientation of cells. Cells react on mechanical stresses and control the remodelling of the tissues composition and mechanical properties [23–26]. Smooth and continuous tubular composite biohybrids can be prepared reliable and are useful for the application in the bioreactor. Even when the PVDF mesh material is used as luminal structure that is not integrated in the tubular wall as seen by others [27–29]. This was done in order to stabilize the tubular structure and to prevent a damage of the gel by the kyphoplasty catheter. Up to date, bioreactors for urological applications can be found nearly exclusively for bladder wall substitutes

of planar scaffold materials. Studies on bladder wall substitutes show benefits with increased cellular proliferation rates for dynamic cultivation conditions, mimicking a physiological intravesical pressure situation [30, 31]. For that reason, planar scaffold materials are deflected frequently. The presented study shows a novel stimulation procedure mimicking a urine bolus in a seamless, tubular scaffold material. Therefore, a kyphoplasty balloon catheter was used to simulate a physiologic movement of a urine bolus. To our knowledge, no comparable bioreactor system can be found in literature.

To date, tubular biohybrids are cultivated and trained in bioreactors, where the cell culture medium is transferred by peristaltic pumps leading to increased intraluminal pressures and diameters [26, 32]. Another method is to stretch ring shaped constructs with hooks [33]. Both methods lead to the same result with circularly arranged cells and improved mechanical properties, which is comparable to the situation in this study.

3 Computational Growth Modelling

The growth of cells in the fibrin tubular structure can be modelled and simulated by using growth theory for soft tissue in which the density is mostly unchanged. In general, growth can be described in different ways. For instance, growth can be an added mass, which can occur through cell division (hyperplasia), cell enlargement (hypertrophy), secretion of extracellular matrix, or accretion at external or internal surfaces. Atrophy (negative growth) can occur through cell death, cell shrinkage, or resorption. In most cases, hyperplasia and hypertrophy are mutually exclusive processes [34]. Depending on the age of the organism and the type of tissue, one of these two growth processes dominates. Furthermore, to fully investigate the tissue growth, remodelling should be considered, especially for medical application such as implants. The remodelling involves changes in material properties. These changes, which often are adaptive, may be brought about by alterations in elastic modulus, internal structure, strength, or mass density. For example, bone and heart muscle may change their internal structures through reorientation of trabeculae and muscle fibres, respectively. In addition, in a weightless environment, bone may lose both stiffness and mass density. Remodelling of biological soft tissue consisting of fibres embedded in a soft matrix (e.g. ureters, arteries and intestines) arises from changes in mechanical properties due to variations in collagen content, reorientation, type of fibres and fibre thickness as well as variations in muscle dimension. However, the model of growth in this paper does not take into account the remodelling for simplification. Herein, the growth is modelled for account the change in shape and mass, the material properties are considered to be only slightly changed and are therefore ignored in the simulation.

In this section, the kinematics and balance laws of finite growth are described. The isotropic growth and transversely isotropic growth are also described and adopted to solve a cube in triaxial tests and a cylinder with an internal pressure. The

simulation results show that the growth models can be applied to simulate the porcine tubular organs in a fibrin-PVDF scaffold. In our approach, the staggered approach in the finite element setting was used.

3.1 Applied Approach

Let Ω_0 be the reference configuration of the body (organ), which is assumed to be stress free. Let us define the deformation map ψ, mapping the reference material point $\boldsymbol{X}$ of a material particle in the configuration Ω_0 to its current point $\boldsymbol{x}$ in the spatial configuration Ω at time t. Then $\mathbf{F} = \mathrm{Grad}\psi(\boldsymbol{X}, \mathrm{t})$ is a material deformation gradient that relates an infinitesimal reference element $\mathrm{d}\boldsymbol{X}$ from Ω_0 to $\mathrm{d}\boldsymbol{x}$ in the deformed configuration Ω_g at time t. In Fig. 4, the intermediate (growth) configuration Ω_g is obtained by instantaneous elastic de-stressing of the current configuration Ω to zero stress [11]. The mass of an infinitesimal volume element in Ω_0 is $\mathrm{d}m_0$. The mass of the corresponding elements in Ω_g and Ω is $\mathrm{d}m$.

The multiplicative decomposition of the deformation gradient into growth $\mathbf{F}_g$ and elastic deformation $\mathbf{F}_e$ [11] is

$$\mathbf{F} = \mathbf{F}_e \cdot \mathbf{F}_g, \qquad \det(\mathbf{F}_g) \neq 1, \det(\mathbf{F}_e) = 1. \tag{1}$$

In (1), $\det(\mathbf{F}_g) \neq 1$ since growth does not require volume preservation [35].

Different from an unchanged mass in the classical continuum mechanics, the mass for a growth object is no longer a conserved quantity. Therefore, transformations of the important quantities of the different configurations must be performed. Herein, the scalar value ρ_0 signifies the reference density of a mass

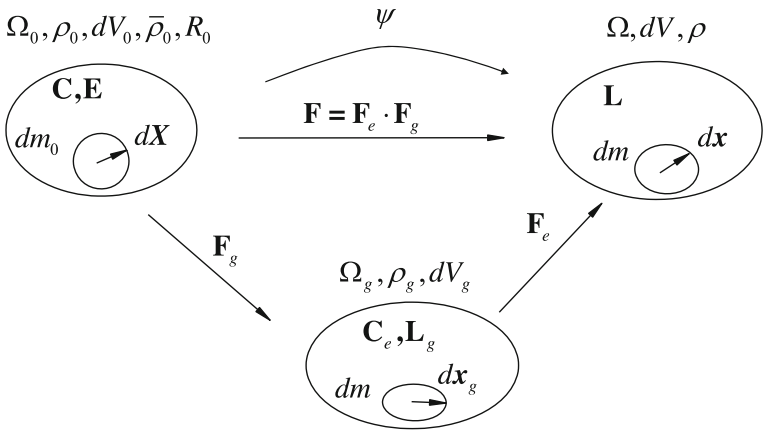

Fig. 4 Multiplicative decomposition of deformation gradient $\mathbf{F}$ into its growth $\mathbf{F}_g$ and elastic $\mathbf{F}_e$ parts

element. Its counterpart in the current and in the growth configurations are denoted by ρ and ρ_g, respectively [12].

A volume element in the reference configuration is $\mathrm{d}V_0$, its counterparts in the current and the growth configurations are $\mathrm{d}V$, and $\mathrm{d}V_g$, respectively. Besides, the Jacobian $J = \det(\mathbf{F}) = \frac{\mathrm{d}V}{\mathrm{d}V_0}$ of the total deformation gradient, the Jacobians J_g and J_e of the growth and the elastic deformation gradients, respectively, are introduced as $J_g = \det(\mathbf{F}_g) = \frac{\mathrm{d}V_g}{\mathrm{d}V_0}$ and $J_e = \det(\mathbf{F}_e) = \frac{\mathrm{d}V}{\mathrm{d}V_g} = \frac{J}{J_g} = \frac{\rho_g}{\rho}$. To model the growth of tissue the governing equations for balance of mass, balance of momentum and density transformation need to be solved.

3.1.1 Balance of Mass

The balance of mass and the balance of momentum for an open system in thermodynamics are universal equations [36]. Thus, both the balance of mass and the balance of momentum must be solved simultaneously or sequentially in growth simulations [37], leading to a requirement of modifying the stiffness matrices. The balance of mass for an open system is

$$\mathrm{Div}\boldsymbol{R} + R_0 = \frac{\mathrm{d}\rho_0}{\mathrm{d}t}, \tag{2}$$

where $\boldsymbol{R}$ is the mass flux vector, R_0 is the mass source per unit volume in the reference configuration. Cell migration can be incorporated phenomenologically through the mass flux $\boldsymbol{R}$. On the other hand, the mass source R_0 can incorporate phenomena such as increased cell growth, cell division or cell enlargement [13]. The balance of mass can be referred to as the 'biological equilibrium' or the 'homeostatic equilibrium' [37]. Without loss of generality, a mass flux through the surface of the considered mass element is neglected in the following discussion [13].

3.1.2 Balance of Momentum

The differential equations of motion are derived from the first Euler's law of motion of the continuum with the usual form as in conventional continuum mechanics with the material divergence [11].

$$\mathrm{Div}(\mathbf{F}\cdot\mathbf{S}) + \rho_0\boldsymbol{b}_0 = \mathrm{Div}\mathbf{P} + \rho_0\boldsymbol{b}_0 = \rho_g^0\frac{\mathrm{dv}}{\mathrm{dt}}, \tag{3}$$

where $\mathbf{S}$ denotes the second Piola-Kirchhoff stress and the nominal stress (first Piola-Kirchhoff stress) $\mathbf{P} = \mathbf{F}\cdot\mathbf{S}$ is related to the nominal traction $\boldsymbol{T}$ by $\boldsymbol{T} = \boldsymbol{N}\cdot\mathbf{P}$, where $\boldsymbol{N}$ is the unit normal vector to the surface Γ_0 bounding the reference volume

Ω_0 and ρ_g^0 is also called the time rate of mass growth per unit reference volume. The nominal traction $\boldsymbol{T}$ is composed of two terms as

$$\boldsymbol{T} = \boldsymbol{T}^{\text{closed}} + \boldsymbol{T}^{\text{open}} \tag{4}$$

in which apart from the classical term in continuum mechanics $\boldsymbol{T}^{\text{closed}}$, the additional growth dependent contribution $\boldsymbol{T}^{\text{open}}$ is taken into account [37]. Similarly, the body force is expressed as

$$\boldsymbol{b}_0 = \boldsymbol{b}_0^{\text{closed}} + \boldsymbol{b}_0^{\text{open}}. \tag{5}$$

The balance of momentum is typically referred to as the 'mechanical equilibrium' [37]. This equation of the open thermodynamic system implies that the growth tensor $\mathbf{F}_g$ (or its determinant J_g) leads to volume changes and in addition causes mass changes. The balance of mass signifies that mass changes result from changes in density represented by the mass flux $\boldsymbol{R}$ and the source R_0 [37].

3.1.3 Density Transformation

The grown mass element dm [12] consists of the reference mass element dm_0 and the mass produced by the mass source R_0 (mass flux $\boldsymbol{R}$ is ignored) during the growth time $[t_0, t]$ as

$$dm = dm_0 + \left(\int_{t_0}^{t} R_0 \mathrm{d}t \right) \mathrm{d}V_0 = \rho_0 \mathrm{d}V_0 + \left(\int_{t_0}^{t} R_0 \mathrm{d}t \right) \mathrm{d}V_0 \tag{6}$$

$\bar{\rho}_0$ is the density in the reference configuration too $\bar{\rho}_0 = \rho_0 + \int_{t_0}^{t} R_0 \mathrm{d}t$.

3.1.4 Essential Balance Equations

The material time derivative of $\bar{\rho}_0$ results in the well-known local balance of mass (continuity equation) in the reference configuration $\dot{\bar{\rho}}_0 = R_0 = r_g^0$, where r_g^0 is also called the time rate of mass growth per unit reference volume [11].

The current form of the continuity equation

$$\frac{\mathrm{d}\rho}{\mathrm{d}t}(\mathrm{d}V) + \rho \frac{\mathrm{d}}{\mathrm{d}t}(\mathrm{d}V) = r_g \mathrm{d}V, \tag{7}$$

where r_g is the time rate of the mass growth per unit current volume [11] and $r_g^0 = J r_g$. For $r_g > 0$ mass growth occurs, and for $r_g < 0$ mass resorption (atrophy or negative growth) takes place.

3.1.5 Density Preservation

The assumption of density preservation from the reference state to the intermediate configuration, i.e. $\rho_0 = \rho_g = \text{const.}$, implies that the volume of the mass element has to change in order to generate a mass change [12]. This effect of a volume change is denoted as growth if the volume increases or as atrophy if the volume decreases [34]. When using the density preservation, the mass source is rewritten as

$$R_0 = J_g \rho_g \mathrm{tr}\mathbf{L}_g = J_g \rho_0 \mathrm{tr}\mathbf{L}_g. \tag{8}$$

where $\mathbf{L}_g$ is the velocity gradient $\mathbf{L}_g = \dot{\mathbf{F}}_g \cdot \mathbf{F}_g^{-1}$ with the material time derivative. Obviously, the mass source can directly be determined if the growth deformation gradient $\mathbf{F}_g$ and its material time rate $\dot{\mathbf{F}}_g$ are given. The density preservation is thus suitable for soft tissues [13].

3.1.6 Constitutive Equations

A mass specific strain energy function $\Phi = \Phi_{\text{iso}} + \Phi_{\text{trans}}$ in terms of the volume specific strain energy functions (W_0, W_g and W) is defined as [38].

$$\Phi = \frac{W_0}{\bar{\rho}_0} = \frac{W_g}{\rho_g} = \frac{W}{\rho} \tag{9}$$

with $W_0\left(\mathbf{F}_e, \mathbf{A}_0^i\right) = J_g W_g\left(\mathbf{F}_g, \mathbf{A}_g^i\right) = JW\left(\mathbf{F}, \mathbf{A}^i\right)$, where W_0, W_g and W are volume specific strain energy functions in the reference, the intermediate and the current configurations, respectively. The elastic strain energy per unit current mass is then given by a function of the elastic Green-Lagrange strain $\mathbf{E}_e$ (or its invariants) and the structure tensors $\mathbf{A}_0^i = \boldsymbol{a}_0^i \otimes \boldsymbol{a}_0^i$, $i = 4, 6$ for the first fibre family and the second fibre family, respectively i.e. $\Phi\left(\mathbf{E}_e, \mathbf{A}_0^i, \bar{\rho}_0\right)$. Generally, the strain energy density functions are usually formulated in terms of the overall deformation gradient $\mathbf{F}$, the growth tensor $\mathbf{F}_g$, the structure tensor $\mathbf{A}_0^i$ and the density $\bar{\rho}_0$ such as $\Phi = W_0\left(\mathbf{F}, \mathbf{F}_g, \mathbf{A}_0^i, \bar{\rho}_0\right)$ [11, 13, 38]. Herein, it is more convenient to manage the strain energy functions which are described in terms of the invariants of the elastic right Cauchy Green tensor $I_1 = \mathrm{tr}(\mathbf{C}_e)$, $I_3 = \det(\mathbf{C}_e)$, where $\mathbf{C}_e = \mathbf{F}_e^T \cdot \mathbf{F}_e$. In this work, the compressible neo-Hookean model was used with the density strain-energy function written as

$$\bar{\rho}_0 \Phi_{\text{iso}}(I_1) = \frac{\mu}{2}(I_1 - 3) - \mu \ln(J_e) + \frac{\lambda}{2}\ln^2(J_e), \tag{10}$$

where $\mu = \frac{E}{2(1+\nu)}$ (with the Poisson's ratio ν) is equivalent to the small strain shear modulus, $\lambda = \frac{E\nu}{(1+\nu)(1-2\nu)}$ is equivalent to the first small strain Lamé's parameter.

$\Phi_{\text{trans}}(I_4)$ is the transversely isotropic strain energy in terms of invariants and can be used to simulate transversely isotropic growth $\left(I_4 = \boldsymbol{a}_0^4 \cdot \mathbf{C}\boldsymbol{a}_0^4\right)$. That means the growth along the fibres dominates others in the rest directions. It is worth noting that a compressible model must be utilized in such a way that the material can grow. Therefore, the volumetric energy, which enforces the incompressibility condition, is ignored.

$$\Phi_{\text{trans}}(I_4) = \frac{k_1}{2k_2}\left\{\exp\left(k_2[I_4 - 1]^2\right) - 1\right\}. \tag{11}$$

The second Piola-Kirchhoff stress tensor in the material configuration is written as

$$\mathbf{S} = 2\frac{\partial W_0}{\partial \mathbf{C}} = 2\bar{\rho}_0 \frac{\partial \Phi}{\partial \mathbf{C}}. \tag{12}$$

Using the push forward operation to the growth configuration on $\mathbf{S}_e$ yields

$$\mathbf{S}_e = \mathbf{F}_g \cdot \mathbf{S} \cdot \mathbf{F}_g^T = 2\bar{\rho}_0 \mathbf{F}_g \cdot \frac{\partial \Phi}{\partial \mathbf{C}} \cdot \mathbf{F}_g^T = 2\bar{\rho}_0 \frac{\partial \Phi}{\partial \mathbf{C}_e} = \mathbf{S}_{e,\text{iso}} + \mathbf{S}_{e,\text{trans}}. \tag{13}$$

The second Piola-Kirchhoff stress for isotropic part is calculated as

$$\mathbf{S}_{e,iso} = 2\bar{\rho}_0 \frac{\partial \Phi(I_1)}{\partial \mathbf{C}_e} = \mu\left(I_1 - \mathbf{C}^{-1}\right) + \lambda \ln(J_e)\mathbf{C}^{-1} \tag{14}$$

and the second Piola-Kirchhoff stress for transversely isotropic part (only one fibre family) is evaluated as

$$\mathbf{S}_{e,\text{trans}} = 2\bar{\rho}_0 \frac{\partial (I_4)}{\partial \mathbf{C}_e} = 2k_1(I_4 - 1)\exp\left(k_2[I_4 - 1]^2\right)\boldsymbol{a}_0^4 \otimes \boldsymbol{a}_0^4. \tag{15}$$

The constitutive tensor $\mathbb{C}$ is then defined as

$$\mathbb{C} = 2\frac{\partial \mathbf{S}_e}{\partial \mathbf{C}_e} = 2\frac{\partial\left(\mathbf{S}_{e,\text{iso}} + \mathbf{S}_{e,\text{trans}}\right)}{\partial \mathbf{C}_e}. \tag{16}$$

The constitutive tensor of the isotropic part is written as

$$\begin{aligned}\mathbb{C}_{iso} = 2\frac{\partial \mathbf{S}_{e,iso}}{\partial \mathbf{C}_e} &= 2\left[-\frac{\partial \mathbf{C}_e^{-1}}{\partial \mathbf{C}_e}\mu + \lambda\left(\frac{\partial \ln J_e}{\partial \mathbf{C}_e} \otimes \mathbf{C}_e^{-1} + \ln J_e \frac{\partial \mathbf{C}_e^{-1}}{\partial \mathbf{C}_e}\right)\right] \\ &= \lambda \mathbf{C}_e^{-1} \otimes \mathbf{C}_e^{-1} + (\mu - \lambda \ln J_e)\mathbb{I}\end{aligned} \tag{17}$$

where $\mathbb{I} = \frac{1}{2}\left(C_{e,IK}^{-1}C_{e,JL}^{-1} + C_{e,IL}^{-1}C_{e,JK}^{-1}\right)$. Similarly, the constitutive tensor of the transversely isotropic part is computed as

$$\begin{aligned}\mathbb{C}_{trans} &= 2\frac{\partial \mathbf{S}_{e,\text{trans}}}{\partial \mathbf{C}_e} \\ &= 4k_1\{\exp\left(k_2[I_4-1]^2\right) + 2k_2(I_4-1)^2\exp\left(k_2[I_4-1]^2\right)(\boldsymbol{a}_0^4 \otimes \boldsymbol{a}_0^4) \otimes (\boldsymbol{a}_0^4 \\ &\quad \otimes \boldsymbol{a}_0^4)\}.\end{aligned} \tag{18}$$

3.2 Computational Growth Models

3.2.1 Isotropic Growth

When considering the smooth muscle cells of porcine tubular organs in a fibrin-PVDF scaffold is isotropic, the isotropic growth model applied in this case is as

$$\mathbf{F}_g = \vartheta \mathbf{I}. \tag{19}$$

Evolution equations for stretch ratios ϑ are given in terms of isotropic scalar functions of the second Piola-Kirchhoff stress tensor $\mathbf{S}_e$ and the right Cauchy-Green strain tensor $\mathbf{C}_e$, assumed to be $\dot{\vartheta} = k_\vartheta(\vartheta)\text{tr}(\mathbf{S}_e \cdot \mathbf{C}_e)$.

To prevent an unlimited growth at an arbitrary nonzero state of stress, it is proposed that during the mass growth [11].

$$k_\vartheta(\vartheta) = k_{\vartheta^0}^+ \left(\frac{\vartheta^+ - \vartheta}{\vartheta^+ - 1}\right)^{m_\vartheta^+}, \tag{20}$$

where $\vartheta^+ > 1$ is the limiting value of the growth stretch ratio. In the case of the mass resorption, the corresponding expression is

$$k_\vartheta(\vartheta) = k_{\vartheta^0}^- \left(\frac{\vartheta - \vartheta^-}{1 - \vartheta^-}\right)^{m_\vartheta^-}. \tag{21}$$

In contrast to [11], we adopt the driving force, which is the Mandel stresses $\mathbf{M}_e = \mathbf{S}_e \cdot \mathbf{C}_e$ [12, 13].

3.2.2 Transversely Isotropic Growth

A transversely isotropic mass growth law is reasonably capable of characterizing a transversely isotropic material, e.g. muscle with a bundle of longitudinal fibres. Therefore, this model can be further employed for the smooth muscle cells of porcine tubular organs in a fibrin-PVDF scaffold due to the experimental data

mentioned above showing the orientation of cells. The unit vector specifying the fibre orientation is denoted by $\boldsymbol{a}_0^4$ in the reference configuration Ω_0. The intermediate configuration Ω_g is defined with the same fiber orientation with respect to the fixed frame of reference. The isotropic growth deformation gradient is defined by assuming that the fibres are embedded in the material [11], this is ensured by defining $\mathbf{F}_g$ such that $\boldsymbol{a}_0^4$ is one of its eigendirections

$$\mathbf{F}_g \cdot \boldsymbol{a}_0^4 = \eta_g \boldsymbol{a}_0^4. \tag{22}$$

An infinitesimal fibre segment in the configuration is parallel to the vector $\boldsymbol{a}^4 = \mathbf{F}_g \cdot \boldsymbol{a}_0^4$, obtained from $\boldsymbol{a}_0^4$ by elastic stretching and rotation [11].

The expression for the growth part of the deformation gradient due to transversely isotropic mass growth [11] is

$$\mathbf{F}_g = \upsilon \mathbf{I} + (\xi - \upsilon) \boldsymbol{a}_0^4 \otimes \boldsymbol{a}_0^4. \tag{23}$$

The Eq. (23) is similar to the transversely isotropic mass growth for orthotropic material, except the direction of $\boldsymbol{a}_0^4$. The difference in growth direction leads to different formulae for the growth stretch ratios. Specifically, $\mathbf{F}_g \cdot \boldsymbol{a}_0^4 = \eta_g \boldsymbol{a}_0^4$ so that the growth stretch ratio in the fibre direction is ξ, while υ is the growth stretch ratio in any orthogonal direction. The inverse of the growth deformation tensor is

$$\mathbf{F}_g^{-1} = \frac{1}{\upsilon}\mathbf{I} + \left(\frac{1}{\xi} - \frac{1}{\upsilon}\right) \boldsymbol{a}_0^4 \otimes \boldsymbol{a}_0^4 \tag{24}$$

$\mathbf{F}_e = \mathbf{F} \cdot \mathbf{F}_g^{-1}$ gives an explicit expression for the elastic part of the deformation gradient

$$\mathbf{F}_e = \frac{1}{\upsilon}\mathbf{F} + \left(1 - \frac{\xi}{\upsilon}\right) \boldsymbol{a}_0^4 \otimes \boldsymbol{a}_0^4. \tag{25}$$

3.2.3 Evolution Equations for Stretch Ratios

The constitutive formulation is completed by specifying appropriate evolution equations for the growth stretch ratios υ and ξ. The evolution equations for the stretch ratios and must be given in terms of isotropic scalar functions of the stress tensor $\mathbf{S}_e$ and the structural tensor $\mathbf{A}_0^4 = \boldsymbol{a}_0^4 \otimes \boldsymbol{a}_0^4$ [11]. The evolution equations of the stretch ratios are assumed to be obtained by including in the list of arguments their current values as

$$\dot{\upsilon} = f_{\upsilon}\left[\xi, \upsilon, S^{e}_{\boldsymbol{a}^4_0}, \frac{1}{2}\left(\mathrm{tr}\mathbf{S}_e - S^{e}_{\boldsymbol{a}^4_0}\right)\right], \tag{26}$$

$$\dot{\xi} = f_{\xi}\left[\xi, \upsilon, S^{e}_{\boldsymbol{a}^4_0}, \frac{1}{2}\left(\mathrm{tr}\mathbf{S}_e - S^{e}_{\boldsymbol{a}^4_0}\right)\right]. \tag{27}$$

The normal component of the second Piola-Kirchhoff stress $\mathbf{S}_e$ in the direction of the fibre is $S^{e}_{\boldsymbol{a}^4_0} = \boldsymbol{a}^4_0 \cdot \mathbf{S}_e \cdot \boldsymbol{a}^4_0$, while $\frac{1}{2}\left(\mathrm{tr}\mathbf{S}_e - S^{e}_{\boldsymbol{a}^4_0}\right)$ represents the average normal stress in the plane perpendicular to the fibre. These two stresses are believed to have a dominant mechanical effect on the transversely isotropic mass growth [11]. Note that the normal stress in the direction of the fibre can be expressed in terms of the Cauchy stress as

$$\boldsymbol{a}^4_0 \cdot \mathbf{S}_e \cdot \boldsymbol{a}^4_0 = J_e\left(\boldsymbol{a}^4_0 \cdot \mathbf{F}_e^{-1}\right) \cdot \boldsymbol{\sigma} \cdot \left(\boldsymbol{a}^4_0 \cdot \mathbf{F}_e^{-1}\right).$$

In the simplest case, the rates of the stretch ratios depend linearly on the stress components, such that

$$\dot{\upsilon} = k_{\upsilon}(\upsilon)\left[S^{e}_{\boldsymbol{a}^4_0} - v_{\upsilon}\left(\mathrm{tr}\mathbf{S}_e - S^{e}_{\boldsymbol{a}^4_0}\right)\right] \tag{28}$$

$$\dot{\xi} = k_{\xi}(\xi)\left[S^{e}_{\boldsymbol{a}^4_0} - v_{\xi}\left(\mathrm{tr}\mathbf{S}_e - S^{e}_{\boldsymbol{a}^4_0}\right)\right] \tag{29}$$

where v_{ξ} and v_{υ} are constants, or functions of ξ and υ. For the sake of simplicity, these constants are chosen as $v_{\upsilon} = v_{\xi} = \frac{1}{2}$.

To prevent an unlimited growth at an arbitrary non-zero state of stress, it is proposed that during mass growth

$$k_{\xi}(\xi) = k^{+}_{\xi^0}\left(\frac{\xi^{+} - \xi}{\xi^{+} - 1}\right)^{m^{+}_{\xi}} \text{ for } S^{e}_{\boldsymbol{a}^4_0} > \frac{v_{\xi}}{1 + v_{\xi}}\mathrm{tr}\mathbf{S}_e \tag{30}$$

$$k_{\upsilon}(\upsilon) = k^{-}_{\upsilon^0}\left(\frac{\upsilon - \upsilon^{-}}{1 - \upsilon^{-}}\right)^{m^{-}_{\upsilon}} \text{ for } S^{e}_{\boldsymbol{a}^4_0} < \frac{v_{\upsilon}}{1 + v_{\upsilon}}\mathrm{tr}\mathbf{S}_e. \tag{31}$$

3.2.4 Numerical Implementation

In isotropic growth case, the constitutive tensor is calculated as

$$\mathbb{C}_e = 2\frac{\mathrm{d}\mathbf{S}_e}{\mathrm{d}\mathbf{C}_e} = 2\left(\frac{\partial \mathbf{S}_e}{\partial \mathbf{C}_e} + \frac{\partial \mathbf{S}_e}{\partial \upsilon} \otimes \frac{\partial \upsilon}{\partial \mathbf{C}_e}\right) = \mathbb{C} + \mathbb{C}_{\upsilon}. \tag{32}$$

In addition, the constitutive tensor of the transversely isotropic growth model is written as

$$\mathbb{C}_e = 2\frac{\mathrm{d}\mathbf{S}_e}{\mathrm{d}\mathbf{C}_e} = 2\left(\frac{\partial \mathbf{S}_e}{\partial \mathbf{C}_e} + \frac{\partial \mathbf{S}_e}{\partial \xi} \otimes \frac{\partial \xi}{\partial \mathbf{C}_e} + \frac{\partial \mathbf{S}_e}{\partial \upsilon} \otimes \frac{\partial \upsilon}{\partial \mathbf{C}_e}\right) = \mathbb{C} + \mathbb{C}_\xi + \mathbb{C}_\upsilon. \tag{33}$$

Note that the elasticity-growth tensor comprises two main parts, the elasticity tensor $\mathbb{C}$ as in the passive response and the active response and the growth tensors $(\mathbb{C}_\xi + \mathbb{C}_\upsilon)$ that relate to remodelling of the material. Furthermore, $(\mathbb{C}_\xi + \mathbb{C}_\upsilon)$ tensors are not symmetric because they are generated from the tensor products of different tensors. Consequently, asymmetric solvers are required for this computation.

The incremental updates for the stretch ratios in the cases of isotropic growth and transversely isotropic growth are presented without loss of generality. Obviously, the strains, the stresses, and the elasticity tensor in (15,17,18) depend on the stretch ratios at any time step. Since (ξ, υ) are introduced as internal variables at integration points, the implicit Euler backward scheme is used to compute the stretch ratios at a time step [37], hence the stretches are formulated as

$$\xi_{n+1} = \xi_n + \dot{\xi}_{n+1}\Delta t \tag{34}$$

$$\upsilon_{n+1} = \upsilon_n + \dot{\upsilon}_{n+1}\Delta t \tag{35}$$

and their derivatives computed as

$$\frac{\partial \xi}{\partial \mathbf{C}_e} = \left(\frac{\partial \dot{\xi}}{\partial \mathbf{C}_e} + \frac{\partial \dot{\xi}}{\partial \xi}\frac{\partial \xi}{\partial \mathbf{C}_e}\right)\Delta t \tag{36}$$

$$\frac{\partial \upsilon}{\partial \mathbf{C}_e} = \left(\frac{\partial \dot{\upsilon}}{\partial \mathbf{C}_e} + \frac{\partial \dot{\upsilon}}{\partial \upsilon}\frac{\partial \upsilon}{\partial \mathbf{C}_e}\right)\Delta t. \tag{37}$$

3.3 Numerical Simulation of Growth

To exhibit the capability of modelling and simulating the growth of cells, a simple test case was investigated with different material laws, such as the neo-Hookean strain energy function and the model in [39]. Their parameters are tabulated in Table 2.

Table 2 Growth parameters for isotropic growth

Mode	$k^+_{\vartheta^0}$	$k^-_{\vartheta^0}$	m^+_ϑ	m^-_ϑ	ϑ^+	ϑ^-	$\triangle t$
Unlimited	1.5×10^{-3}	0.8×10^{-3}	2.5	3	2	0.5	1
Limited	6.5×10^{-3}	0.8×10^{-3}	1.5	3	1.24	0.5	1

It is well known that soft tissues are considered as nearly incompressible materials. However, the tissues grow under stress induced changes, and hence, the incompressibility condition need not strictly be imposed. Thus, the Poisson's ratio is chosen as $v = 0.4$.

3.3.1 Triaxial Tension and Compression Tests of a Cube

The cube is subjected to monotonic loading by prescribed displacements as in the training described above for the tubular fibrin structure. Loading can be simultaneously applied (e.g. in a step function with 5 times increments) along three orthogonal directions of one eighth of the cube since the intermediate configuration (growth configuration) is incompatible, see Fig. 5. The cube is simulated by finite elements using the hexahedral element (FEM-H8). The time step Δt (its unit depends on the unit of the measurements of the growth process or time counted for tissue enlargement, e.g. when this time is measured in hour or day, then Δt is measured in the same unit) found for each load increment are solved at the biological equilibrium state (all stresses are zero). Figure 5 clearly shows the numerical results of employing the neo-Hookean model with the shear modulus $\mu = 1.5$ kPa. The larger stresses $\boldsymbol{\sigma}$ induce the smaller number of time steps, i.e. the tissue grows faster. Correspondingly, the stresses in each load increment are decreasing slowly, see Fig. 5. At the final state, the increased volume of the cube is 3.375 times the initial volume. In this case, there is no growth limit since the load (prescribed displacement) is 1.4 times smaller than the limit stretch ratio $\vartheta^+ = 2.0$.

In contrast with the tension test, in the simulations of the compression test, there are reductions of the size of the cube that were compensated by the negative growth (Fig. 6) and the larger strain leading to a faster atrophy. The anisotropic material

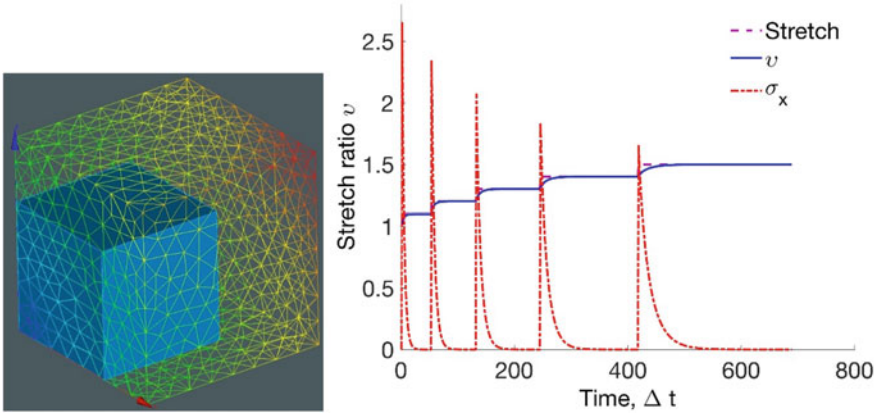

Fig. 5 Stretch and growth stretch ratio for a cube in tension test [40]

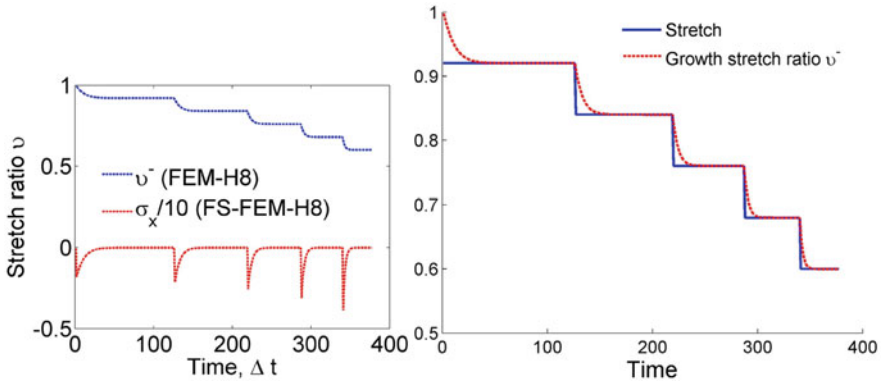

Fig. 6 Stretch and stretch ratio for cube of isotropic tissue in compression test [40]

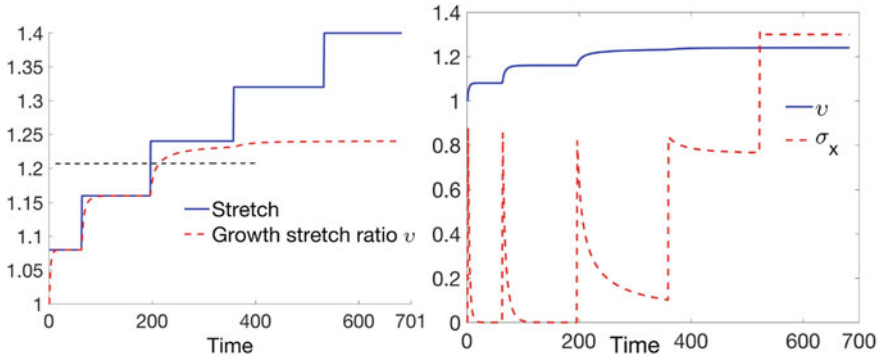

Fig. 7 Stretch and growth stretch ratio for a cube of anisotropic tissue in tension test with limit constant [40]

described in [39] and the growth constants in Table 2 adopted for limit growth simulation, result in residual stresses which cannot be compensated by growth in Fig. 7.

3.3.2 Tube Tension Test

For the first step of mimicking approximately urine dropping inside the ureter, an extension along axial direction of a tube was performed to investigate the growth of the tube, see Fig. 8 (left). The isotropic growth parameters are the same as in the case of the triaxial test, but the material model is transversely isotropic (11), combined with the neo-Hookean material with constants as $\mu = 1.28$ kPa, $k_1 = 1.00$ kPa, $k_2 = 1.91$, and the vector $\boldsymbol{a}_0^4 = [100]^{\mathrm{T}}$. The FEM boundary conditions

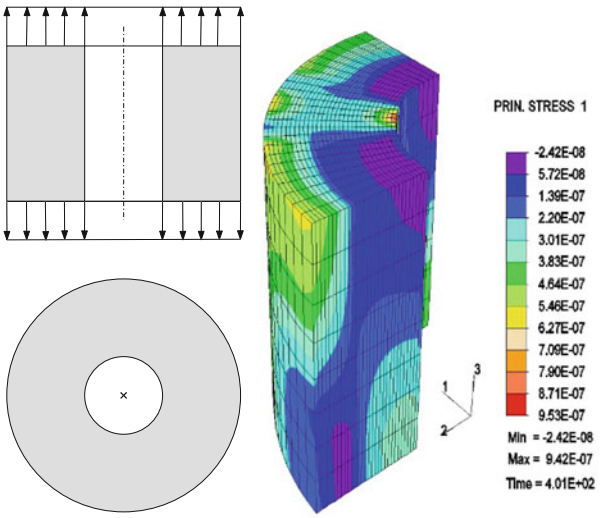

Fig. 8 Extension of a tube: boundary conditions and major principal stress [40]

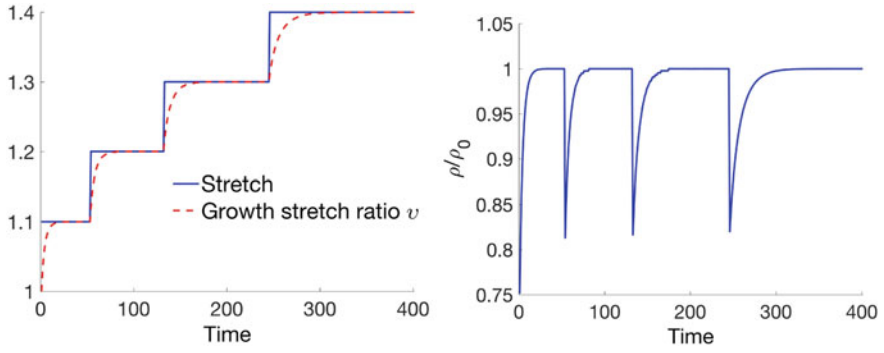

Fig. 9 FEM result of growth of extension of a tube [40]

and the major principal stress approaching zero are depicted in Fig. 8 in which we prescribe both ends of the tube with a specified stretch. For each increasing stretch imposed, the tissue needs to grow in order to compensate the imposed stretch to reach the zero-stress state. Specifically, Fig. 9 shows that after reaching the stretch of 1.4 with four loading increments, the first principal stress becomes zero due to compensation by growth with the density ratio approaching unity for the density preservation case. At the beginning of each stretch prescribed, the density curve drops suddenly and gradually increases to the magnitude of one. Consequently, the tube enlarges both in the radial and the longitudinal directions with a maximal stretch ratio of 1.4.

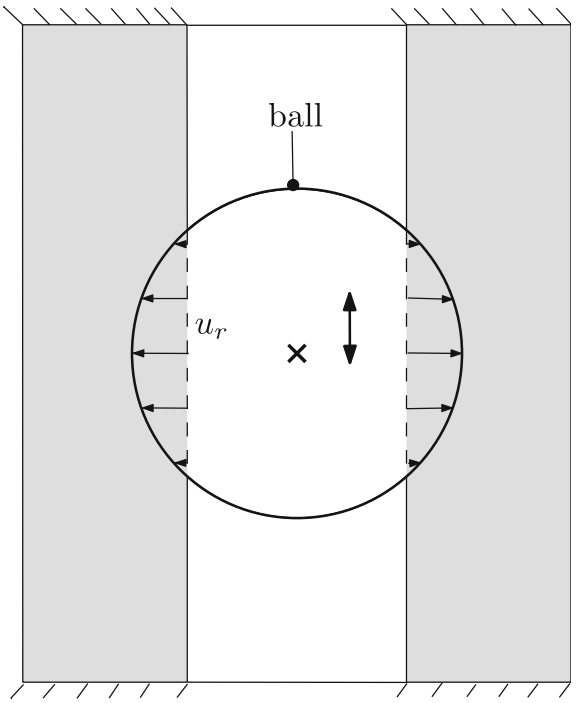

Fig. 10 Balloon travelling inside a tube mimicking urine drop in a fibrin-PVDF scaffold

Figure 10 describes the mimicking of urine with a ball or a hyperelastic kyphoplasty balloon catheter travelling inside the muscle in fibrin-PVDF scaffold. This is future work of the study applied to transversely isotropic growth and transversely isotropic material. This case is a dynamic simulation since the ball inducing displacement u_r, travels along the axial direction of the tube modelled as transversely isotropic. Hence, the growth of tissue will be solved and can be compared with experimental data such as the mechanical properties, shape, size and fibre orientation of the smooth muscles in a fibrin-PVDF scaffold.

4 Conclusions

Our work presents a novel stimulation procedure mimicking a urine bolus, applied to smooth muscle cells of porcine tubular organs in a fibrin-PVDF scaffold. The mechanical stimulation has a tendency to increase mechanical stability for stimulated prostheses. A similar tendency was observed for extended incubation periods. The rupture pressure is also increased after two weeks of incubation with mechanical stimulation. Furthermore, the stimulation results in a preferred orientation of cells along the tubular structure of the prosthesis. However, the intensity of

mechanical stimulation is dependent on various parameters and different models: the applied cell type, cell source, cell passage as well as in the experimental setup. Nevertheless, it is seen to be stress level and cell type specific.

In this study, we focus on the change in shape and mechanical properties of cells with stimulated prostheses so that the growth theory can be applied to simulate the experiments. Although, growth is generally a very complex process and can account for the increase of tissue volume of inner organs due to daily activities and gravity this process can be characterised by simulation. With the mechanical stimulation presented for the experiments on smooth muscle cells of porcine tubular organs in a fibrin-PVDF scaffold, the isotropic and transversely isotropic growth models are certainly adequate for simulating the growth of smooth cells. Consequently, a standard protocol can be applied to conduct experiments and growth simulations are adopted to validate simulations with experimental data. That can be a novel challenge for the future work.

Acknowledgements The focal cyclic intraluminal mechanical stimulation is based on suggestions by G. M. Artmann. This project was supported in part by the German Federal Ministry of Education and Research of Germany through the FHprofUnt project "BINGO" (03FH073PX2) and by the German Federal Ministry of Economics and Technology through the project "UREPLACE" (KF0634101SB8).

Conflict of Interest

The authors declare that they have no conflict of interest.

References

1. Taulbut, M., Walsh, D., McCartney, G., Parcell, S., Hartmann, A., Poirier, G., et al. (2014). Spatial inequalities in life expectancy within postindustrial regions of Europe: A cross-sectional observational study. *BMJ Open, 4*(6), 1–9 (e004711).
2. Wohland, P., Bees, P., Gillies, C., Alvanides, S., Matthews, F. E., O'neil, V., et al. (2014). Drivers of inequality in disability-free expectancy at birth and age 85 across space and time in Great Britain. *Journal of Epidemiology and Community Health, 68,* 826–833.
3. Shalhav, A. L., Elbahnasy, A. M., Bercowsky, E., Kovacs, G., Brewer, A., Maxwell, K. L., et al. (1999). Laparoscopic replacement of urinary tract segments using biodegradable materials in a large-animal model. *Journal of Endourology, 13,* 241–244.
4. El-Assmy, A., El-Sherbiny, A. T., El-Hamid, M. A., Mohsen, T., Nour, E. M., Bazeed, M., et al. (2004). Use of single layer small intestinal submucosa for long segment ureteral replacement: A pilot study. *The Journal of Urology, 171,* 1939–1942.
5. Seifarth, V., Grosse, J. O., Gossmann, M., Janke, H. P., Arndt, P., Koch, S., et al. (2017). Mechanical induction of bi-directional orientation of primary porcine bladder smooth muscle cells in tubular fibrin-poly(vinylidene fluoride) scaffolds for ureteral and urethral repair using cyclic and focal balloon catheter stimulation. *Journal of Biomaterials Applications, 32*(3), 321–330.

6. Filippo, R. E. D., Yoo, J. J., & Atala, A. (2002). Urethral replacement using cell seeded tubularized collagen matrices. *The Journal of Urology, 168,* 1789–1793.
7. Orabi, H., AbouShwareb, T., Zhang, Y., Yoo, J. J., & Atala, A. (2013). Cell-seeded tubularized scaffolds for reconstruction of long urethral defects: A preclinical study. *European Urology, 63,* 531–538.
8. Huang, A. H., & Niklason, L. E. (2011). Engineering biological-based vascular grafts using a pulsatile bioreactor. *Journal of visualized experiments: JoVE, 52,* 1–14.
9. Fu, Q., Deng, C. L., Zhao, R. Y., Wang, Y., & Cao, Y. (2014). The effect of mechanical extension stimulation combined with epithelial cell sorting on outcomes of implanted tissue-engineered muscular urethras. *Biomaterials, 35,* 105–112.
10. Rodriguez, E. K., Hoger, A., & McCulloch, A. D. (1994). Stress-dependent finite growth in soft elastic tissues. *Journal of Applied Biomechanics, 27*(4), 455–467.
11. Lubarda, V. A., & Hoger, A. (2002). On the mechanics of solids with a growing mass. *International Journal of Solids and Structures, 39,* 4627–4664.
12. Himpel, G., Kuhl, E., Menzel, A., & Steinmann, P. (2005). Computational modelling of isotropic multiplicative growth. *Computer Modeling in Engineering & Sciences, 8,* 119–134.
13. Kuhl, E., Mass, R., Himpel, G., & Menzel, A. (2006). Computational modeling of arterial wall growth. *Biomechanics and Modeling in Mechanobiology, 6,* 321–331.
14. Holzapfel, G. A. (2000). *Nonlinear solid mechanics, a continuum approach for engineering*. Chichester: Wiley.
15. Montzka, K., Läufer, T., Becker, C., Grosse, J., & Heidenreich, A. (2011). Microstructure and cytocompatibility of collagen matrices for urological tissue engineering. *BJU International, 107,* 1974–1981.
16. Cornelissen, C. G., Dietrich, M., Krüger, S., Spillner, J., Schmitz-Rode, T., & Jockenhoevel, S. (2012). Fibrin gel as alternative scaffold for respiratory tissue engineering. *Annual Review of Biomedical Engineering, 40,* 679–687.
17. Dellenback, R. J., & Chien, S. (1970). The extinction coefficient of fibrinogen from man, dog, elephant, sheep, and goat at 280 mμ. *Proceedings of the Society for Experimental Biology and Medicine, 134,* 353–355.
18. Cholewinski, E., Dietrich, M., Flanagan, T. C., Schmitz-Rode, T., & Jockenhoevel, S. (2009). Tranexamic acid—An alternative to aprotinin in fibrin—Based cardiovascular tissue engineering. *Tissue Engineering Part A, 15,* 3645–3653.
19. Eyrich, D., Brandl, F., Appel, B., Wiese, H., Maier, G., & Wenzel, M. (2007). Long-term stable fibrin gels for cartilage engineering. *Biomaterials, 28,* 55–65.
20. Dorothea, L., Stollenwerk, K., Seifarth, V., Zraik, I. M., Vogt, M., Srinivasan, P. K., et al. (2016). Two differentially structured collagen scaffolds for potential urinary bladder augmentation: Proof of concept study in a Göttingen minipig model. *Journal of Translational Medicine, 15,* 1–16.
21. Seifarth, V. (2015). *Ureteral tissue engineering: Development of a bioreactor system and subsequent characterization of the generated biohybrids* (PhD Dissertation). University Duisburg-Essen, Germany.
22. Ternifi, R., Gennisson, J. L., Tanter, M., & Beillas, P. (2013). Effects of storage temperature on the mechanical properties of porcine kidney estimated using Shear Wave Elastography. *Journal of the Mechanical Behavior of Biomedical Material, 28,* 86–93.
23. Janmey, P. A., & McCulloch, C. A. (2007). Cell mechanics: Integrating cell responses to mechanical stimuli. *Annual Review of Biomedical Engineering, 9,* 1–34.
24. Murphy, S. V., & Atala, A. (2013). Organ engineering—Combining stem cells, biomaterials, and bioreactors to produce bioengineered organs for transplantation. *BioEssays, 35,* 163–172.
25. Nishi, M., Matsumoto, R., Dong, J., & Uemura, T. (2013). Engineered bone tissue associated with vascularization utilizing a rotating wall vessel bioreactor. *Journal of Biomedical Materials Research—Part A, 101*, 421–427.

26. Seliktar, D., Black, R. A., Vito, R. P., & Nerem, R. M. (2000). Dynamic mechanical conditioning of collagen-gel blood vessel constructs induces remodeling in vitro. *Annual Review of Biomedical Engineering, 28,* 351–362.
27. Tschoeke, B., Flanagan, T. C., Cornelissen, A., Koch, S., Roehl, A., Sriharwoko, M., et al. (2008). Development of a composite degradable/nondegradable tissue-engineered vascular graft. *Artificial Organs, 32,* 800–809.
28. Jockenhoevel, S., & Flanagan, T. C. (2011). In D. Eberli (Ed.), *Tissue engineering for tissue and organ regeneration*. InTech.
29. Geutjes, P., Roelofs, L., Hoogenkamp, H., Walraven, M., Kortmann, B., de Gier, R., et al. (2012). Tissue engineered tubular construct for urinary diversion in a preclinical porcine model. *The Journal of Urology, 188,* 653–660.
30. Wei, X., Li, D. B., Xu, F., Wang, Y., Zhu, Y. C., Li, H., et al. (2011). A novel bioreactor to simulate urinary bladder mechanical properties and compliance for bladder functional tissue engineering. *Chinese Medical Journal (Engl), 124,* 568–573.
31. Davis, N. F., Mooney, R., Piterina, A. V., Callanan, A., McGuire, B. B., Flood, H. D., et al. (2011). Construction and evaluation of urinary bladder bioreactor for urologic tissue-engineering purposes. *Urology, 78,* 954–960.
32. Wang, C., Cen, L., Yin, S., Liu, Q., Liu, W., Cao, Y., et al. (2010). A small diameter elastic blood vessel wall prepared under pulsatile conditions from polyglycolic acid mesh and smooth muscle cells differentiated from adipose-derived stem cells. *Biomaterials, 31,* 621–630.
33. Kanda, K., Matsuda, T., & Oka, T. (1993). Mechanical stress induced cellular orientation and phenotypic modulation of 3-D cultured smooth muscle cells. *ASAIO Journal, 39*(3), M668–M690.
34. Taber, L. A. (1998). Biomechanical growth laws for muscle tissue. *Journal of Theoretical Biology, 193,* 201–213.
35. Humphrey, J. D. (2002). *Cardiovascular solid mechanics-cells, tissues, and organs*. New York: Springer.
36. Kuhl, E. (2004). *Theory and numerics of open system continuum thermodynamics-Spatial and material settings* (Habilitation thesis). Technical University of Kaiserslautern, Germany.
37. Kuhl, E., Menzel, A., & Steinmann, P. (2003). Computational modeling of growth: A critical review, a classification of concepts and two new consistent approaches. *Computational Mechanics, 32,* 71–88.
38. Menzel, A. (2007). A fibre reorientation model for orthotropic multiplicative growth: Configurational driving stresses, kinematics-based reorientation, and algorithmic aspects. *Biomechanics and Modeling in Mechanobiology, 6,* 303–320.
39. Duong, M. T., & Staat, M. (2014). A face-based smoothed finite element method for hyperelastic models and tissue growth. In E. Oñate, J. Oliver & A. Huerta (Eds.), *Proceedings 11th World Congress on Computational Mechanics (WCCM XI), 5th European Conference on Computational Mechanics (ECCM V), 6th European Conference on Computational Fluid Dynamics (ECFD VI)* (pp. 2657–2668), Barcelona, Spain.
40. Duong, M. T. (2014). *Hyperelastic modeling and soft-tissue growth integrated with the smoothed finite element method—SFEM* (PhD Dissertation). RWTH Aachen University, Germany.

Author Biography

Minh Tuấn Dương (Vietnam), Dr. Ing. He is a lecturer of Hanoi University of Science and Technology. He was a researcher and postdoc at the Biomechanics Laboratory of the Institute for Bioengineering at Aachen University of Applied Sciences, focusing on biomechanical modelling and simulation of hyper-elastic materials using the finite element method (FEM) and Smoothed FEM (SFEM). He received his doctoral degree in mechanical engineering in 2014 at RWTH Aachen University, Germany. Currently, he is a postdoctoral researcher at the University of Erlangen-Nuremberg with a topic on modelling and simulation of a heart support system.